2014-07-21

Optical Properties Measurements of Rat Muscle and Myocardium at 980 and 1860 nm Using Single Integrating Sphere Technique

Mohamed Abdulrahman Almadi
mohalmadi@ksu.edu.sa

UNIVERSITY OF MIAMI

OPTICAL PROPERTIES MEASUREMENTS OF RAT MUSCLE AND
MYOCARDIUM AT 980 AND 1860 nm USING SINGLE
INTEGRATING SPHERE TECHNIQUE

By

Mohamed Almadi

A THESIS

Submitted to the Faculty
of the University of Miami
in partial fulfillment of the requirements for
the degree of Master of Science

Coral Gables, Florida

August 2014

UNIVERSITY OF MIAMI

A thesis submitted in partial fulfillment of
the requirements for the degree of
Master of Science

OPTICAL PROPERTIES MEASUREMENTS OF RAT MUSCLE AND
MYOCARDIUM AT 980 AND 1860 nm USING SINGLE
INTEGRATING SPHERE TECHNIQUE

Mohamed Almadi

Approved:

_____
Suhrud M. Rajguru, Ph.D.
Assistant Professor of Biomedical
Engineering and Otolaryngology

_____
Jorge Bohorquez, Ph.D.
Associate Professor in Practice, Biomedical
Engineering

_____
Nelson Salas, Ph.D.
Research Assistant Professor, Biomedical
Engineering

_____
M. Brian Blake, Ph.D.
Dean of the Graduate School

ALMADI, MOHAMED   (M.S., Biomedical Engineering)

<u>Optical Properties Measurements of Rat</u>   (August 2014)
<u>Muscle and Myocardium at 980 and</u>
<u>1860 nm Using Single Integrating</u>
<u>Sphere Technique</u>

Abstract of a thesis at the University of Miami.

Thesis supervised by Suhrud M. Rajguru, Ph.D., and Nelson Salas, Ph.D.
No. of pages in text. (50)

The optical properties of a rat muscle and myocardium were measured at two wavelengths 980 and 1860 nm. The tissues used in this experiment were fresh and sliced to a specific thickness of 600 µm. A single integrating sphere system was used to determine the diffuse reflectance, diffuse transmittance, and collimated transmittance of these tissue samples. An inverse Monte Carlo algorithm was then used to calculate the optical properties from the measurements obtained from the single integrating sphere system. The system was calibrated and validated by using distilled water. The absorption coefficient of the rat's muscles was found to be greater at 1860 nm than at 980 nm. At 980 and 1860 nm, the mean absorption coefficient over 6 samples was 0.182 mm^{-1} and 1.9785 mm^{-1} respectively. At 980 and 1860 nm the mean absorption coefficient over 6 samples of the rat's myocardium was 0.6263 mm^{-1} and 1.6370 mm^{-1} respectively. The results showed that there is an increase in absorption in 1860 nm, which follows the general trend of water absorption spectra. Identifying the optical properties is a key step to understanding the mechanism behind photostimulation.

Acknowledgments

I would like to express my deepest gratitude to my advisor, Dr. Suhrud Rajguru for his help and guidance throughout this project. I would like to thank my co-advisor Dr. Nelson Salas for providing me with the tools to finish this thesis. Special thank goes to Dr. Jorge Bohorquez for serving as a member on my thesis committee. I would like to thank my colleague Weitao Jiang for his great assistance with the laboratory work.

Many thanks go to my wife Rawan and my friend Ahmad Alokaily. They were always supporting me and encouraging me with their best wishes. Finally, I would like to thank my parents. They were always cheering me up through the good and bad times.

TABLE OF CONTENTS

LIST OF TABLES

LIST OF FIGURES

Chapter 1: Introduction and Goals

Two centuries ago, Luigi Galvani discovered that electrical pulses cause muscle spasms when he was performing an experiment on a frog's leg (Parent 2004). Since then, electrical pulses have been used to stimulate neurons. Despite the success of this method for stimulation, there are limitations caused by the interaction between the electrode and the targeted tissue. High current levels can cause chemical reactions and that will lead to tissue damage. Furthermore, there is potential mechanical damage to the tissue where the stimulation electrode is placed. The neural responses are often hard and difficult to measure when an electrical stimulation is used because the magnitude of the electrical stimulation is much higher than the neural responses. To circumvent these limitations, optical stimulation has been introduced as a new method for stimulation.

Optical stimulation of the excitable tissues is a new therapeutic approach in the medical field in which excitable tissue is stimulated by light-tissue interaction. Optical stimulation can be achieved by using several methods such as caged neurotransmitters, optogenetics, or lasers. Laser stimulation has been used in several studies. Arvanitki and Chalazonitis used visible or near infrared light to quantify the effects on isolated various nerves (Arvanitaki & Chalazonitis 1961). Fork used a continuous-wave 488 nm wavelength laser to irradiate photosensitive Aplysia cells without causing any damage to the neural cells (Fork 1971). In 1988 Wade et al discovered that there is a significant increase in neurotransmitters in cells after irradiation with tungsten lamp compared to the non-irradiant ones (Wade et al., 1988). Another group used near infrared laser to measure pulsed optical stimulation in brain slices. Their results showed that there is a probability of generating action potential when the tissue is irradiated with light (Hirase et al., 2002).

A recent study demonstrated that pulsed infrared (IR) laser could stimulate rat sciatic nerve. Moreover, mid infrared wavelengths (2 – 6μm) can cause nerve stimulation without any ablation side effects (Wells et al., 2005). In 2006, a study found that it is possible to stimulate the auditory nerve with a 2120 nm Holmium:YAG laser. They found that stimulating with optical radiation would not cause any neural damage, even when stimulating for several hours (Izzo et al., 2006). Another study used short pulses of IR (1863 nm) on cardiac muscles. The results showed that, at 1863 nm, the cardiac cells started to evoke action potentials (Dittami et al., 2011).

These studies prove that IR laser light can be used to stimulate excitable tissue, such as nerves and cardiac muscles. However, these studies only demonstrate that they can excite this tissue without studying the mechanism behind that. The laser light propagation within these tissues at the resulting laser-tissue interaction must be understood to efficiently utilize IR laser radiation to stimulate excitable tissue without causing undesired damage. This laser light propagation and resultant laser-tissue interaction cannot be determined without knowledge of the optical properties of the excitable tissue. The goal of this study is to measure and study the optical properties of rat muscle and myocardium at 980 nm and 1860 nm.

Chapter 2: Background

2.1 General Anatomy and Physiology:

2.1.1 The Somatic Motor System:

Muscle cells generate most of the primitive animal movements. Generally, there are three types of muscle cells depending on the appearance of the cells under the microscope: smooth, cardiac, and skeletal muscles. Smooth muscles are responsible for internal actions such as blood flow and the movement of the intestines. Cardiac muscle is exclusively responsible for pumping blood. Skeletal muscles are primarily responsible for bone movement around joints, which eventually cause body movement (Kandel et al., 2000). These types of muscles and the nervous system that controls them are collectively called the somatic nervous system (Bear et al., 2007).

Innervation of the somatic motor system depends on the type of the muscle. Smooth muscles are innervated by the autonomic nervous system (ANS). The cardiac muscles do not need any innervation because it generates its own stimulation. However, the autonomic nervous system (ANS) controls the acceleration and deceleration of the heart rate. Skeletal muscles, on the other hand, are innervated by the central nervous system (CNS).

2.1.2 Muscle Fiber Structure:

Typical muscle consists of parallel bundles of straight fascicles. These fascicles are divided into smaller cells called muscle fibers. These fibers are subdivided into smaller cylindrical structure called myofibrils. Each myofibril is surrounded by sarcoplasmic reticulum and t tubule. Sarcoplasmic reticulum (SR) is an intracellular

extensive sac filled with Ca^{2+}. T tubule is a network of tunnels that connect the action potential from the sarcolemma to the sarcoplasmic reticulum. Muscle fibers are covered by sarcolemma, which is an excitable cell membrane. The structure of a muscle fiber is shown in figure 2.1 (Bear et al., 2007). One of the differences between cardiac and skeletal muscles is the number of mitochondria.
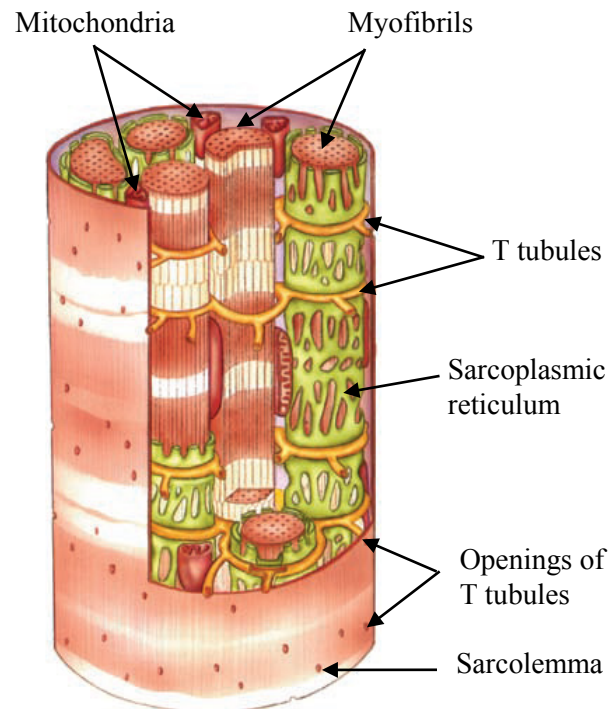
Figure 2.1: The structure of a muscle fiber. The muscle fiber contains a bundle of myofibrils. Each myofibril is surrounded with Sarcoplasmic reticulum (SR) and t tubules. Sarcolemma membrane encloses the muscle fiber form outside. (Bear et al., 2007).

2.2 Stimulating Excitable Cells:

2.2.1 Electrical Stimulation:

Electrical stimulation uses electrical current to stimulate excitable cells. Even though electrical stimulation has been a valuable tool to stimulate cells, it is still has some limitations. It is difficult to stimulate selective parts of the tissue when using electrical stimuli. The electrode should be in a direct contact with the tissue, which can cause

damage to the tissue. The damage can be caused by either the physical contact with the electrode or by the large current generated near the location where the electrode is placed. To overcome these limitations, studies started to use photostimulation.

2.2.2 Photostimulation:

In this type of stimulation a light beam, delivered via optical fiber, is used as a stimulus. Since the stimulus is delivered in a noncontact manner, the damage of the tissue due to direct contact is eliminated. Unlike electrical stimulation, photostimulation can be focused into a small area, giving the ability for higher spatial selectivity (Rajguru et al., 2010).

In 1971, Richard Fork used 488 nm laser light to evoke action potential in ganglion cells of an Aplysia (Fork 1971). Since then, several groups have developed this technique. Photostimulation can be achieved through different approaches: light-mediated uncaging of signaling molecules, photogenic stimulation, and photostimulation by using IR laser.

a) Light-mediated Uncaging of Signaling Molecules

This method uses caged compounds as a carrier to the neurotransmitter. These compounds are artificial molecules that are controlled and activated by light. The name of these molecules comes from the concept that small signaling molecules can be trapped inside a membrane that can only be dismembered by light. The biomolecule should be inactive in the caged status. Upon illumination with a specific wavelength, the caging group should release the biomolecule in a sufficient speed. The only photoproduct that is allowed to interact with the biological system is the caged transmitters (Adams & Tsien

1993). When the caged compound is activated, the active neurotransmitter will be released resulting an increase in neurotransmitters in this specific area and eventually cause stimulation to the cell.

b) Optogenetic Stimulation

Cells are genetically modified to be more sensitive to light. These modifications target some of the light-sensitive ion gates found on the cell membrane to be sensitive to a specific wavelength. Interestingly, this approach can be used in both stimulation and inhabitation applications. This approach has been used in both *in vitro* and *in vivo*. (McGovern et al., 2010).

c) Photostimulation

Using monochromatic light for stimulation has been used in several studies. Arvanitki and Chalazonitis used visible or near infrared to quantify the effects on isolated various nerves (Arvanitaki & Chalazonitis 1961). Fork used continues 488 nm wavelength laser to irradiate photosensitive Aplysia neural cells without causing any damage to them (Fork 1971). Another group used near infrared laser to measure pulsed optical stimulation in brain slices. Their results showed that there is a probability of generating action potential when the tissue is irradiated by light (Hirase et al., 2002). A recent study demonstrated that pulsed infrared laser could stimulate rat sciatic nerve. Moreover, mid infrared wavelengths (2 – 6μm) can cause nerve stimulation safely and without ablation (Wells et al., 2005).

The stimulation mechanism behind photostimulation is still unknown. There are various effects that might occur when a laser beam interacts with the tissue. This reaction

might happen as a photochemical, photothermal, photomechanical, or electric field effects. However, studies (Jacques 1992, Thomsen 1991, Wells et al., 2007) investigated the biophysical mechanisms responses to laser-tissue interaction. Their results eliminated the possibility that photochemical, electric field effects, and photomechanical can explain the stimulation mechanism. However, photothermal mechanism is the most likely mean of stimulation. The photothermal response is basically the development of heat within the tissue by the absorption of the radiation energy. This transformation of energy mediates an unknown secondary mechanism (Rajguru et al., 2010).

Even though photostimulation has been successfully used to stimulate biological cells in several studies, the mechanism behind the stimulation is unidentified. It seems that the photothermal effect is the most possible cause of the stimulation; yet, the exact mechanism is unknown.

Knowing the amount of energy absorbed and the way laser propagates through the tissue will clarify the photothermal effect. The first step to obtain this information is measuring the optical properties of the tissue. Also, any external stimulation may cause damage to the applied area. Therefore, it is important to know the effect of each stimulus and how to control it.

2.3 Tissue Optical Properties:

When light propagates through a tissue it will interact with its molecular structures. Biological tissue is generally considered an inhomogeneous medium since it contains different structures and organelles. Since biological tissue generally is a turbid medium, the propagation of light will be both absorbed and scattered. The power density, or intensity of the light, the irradiation time, and the optical properties of the tissue

determines the light interaction with any specific molecular structure. Tissue optical properties include the refractive index (n), absorption coefficient (μ_a), scattering coefficient (μ_s), and the anisotropy coefficient (g). The refractive index will determine the amount of light reflected or transmitted off its boundaries, while the others determine the amount of light absorption, scattering, and scattering anisotropy at a specific location within the tissue.

2.3.1 Refractive Index (n):

Refractive index (n) determines the direction and speed of light in the medium once the light has crossed its boundary. Any changes in the refractive indices will abrupt the direction of the incident light. When the light refracts with a medium of a different refractive index at its boundary and at an incident angle relative to the normal of the boundary, it will travel in a different direction (Figure 2.3). Any changes in the refractive index gives rise to refraction, reflection, and scattering. The refractive index can be calculated by using the following equation:

$$n = c_{vacuum} / v \hspace{3cm} \text{Equation (2.1)}$$

where (c_{vacuum}) is the speed of light in vacuum, (v) is the speed of light in the medium.
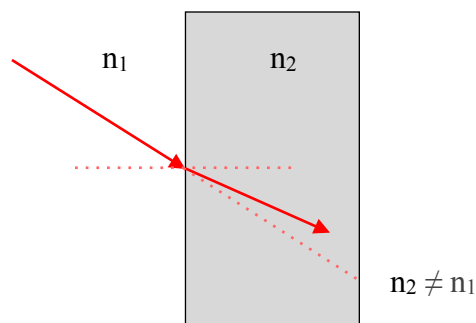
Figure 2.2: The refractive index determines the direction and speed of the propagated light.

2.3.2 Absorption:

When a light photon propagates within tissue, some of its energy will be transferred to the surrounding molecules and will produce some sort of excitation. This transfer of energy is known as absorption. Absorption depends on the wavelength of the light used and the absorption coefficient of the targeted tissue. The absorption coefficient describes the probability of photon absorption per unit path length (mm^{-1}) and it can be calculated by using Lambert-Beer law for non-scattering medium:

$$I = I_0 \, e^{-\mu_a \, d}$$
Equation (2.2)

where (I) is the light intensity reduced by the absorption, (I_0) is the initiated light intensity, (μ_a) is the absorption coefficient, and (d) is the distance the light traveled in the medium or the thickness of the tissue sample (figure 2.3).

Molecules that absorb light are called photoacceptors. Within each photoacceptor there are particular moiety responsible for the absorption of light known as chromophores. Chromophores are either organic cofactors or metal ions and usually found within a protein structure. These chromophores contain electrons that can be excited. The excitation of these electrons from ground state to excitation state will induce molecular changes (Gonzalez et al., 2014).
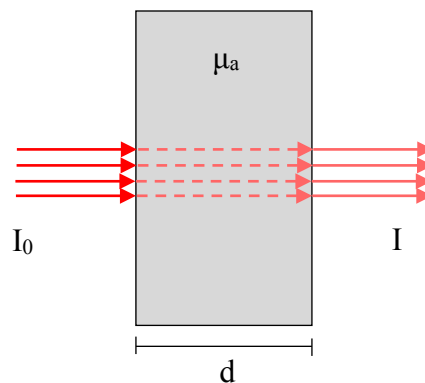
Figure 2.3: The absorption phenomenon. I_o is the incident intensity, I is the final intensity after absorption, d is the thickness, μ_a is the absorption coefficient.

The main chromophores found in biological tissue are water, lipids, proteins, and hemoglobin. Water, proteins, and lipids remain constant over time, but on the other hand, the absorption of the hemoglobin changes according to whether it is oxygenated or deoxygenated (Schmidt 2000). Every chromophore has its unique absorption characteristics in different wavelengths.

a) Water

The chemical substance found most in the human body is water, accounting for up to 75% of the body mass. The water content depends on the tissue type, age, and gender. For example, the brain of a newborn baby contains 90% water but this percentage drops to 74% in adults (White at al., 1991). Because it has a high concentration in tissues (Figure 2.4), water is considered as one of the most important chromophore in the tissue especially within the IR region (Hollis 2002).

b) Lipids

Neutral fats are the most common form of lipids, and it is usually found in subcutaneous tissues and around the organs. The main component of the cell membrane is another type of lipids called phospholipids. The percentage of lipid in the human body varies with age and gender (White at al., 1991). Figure 2.5 shows the absorption spectrum of lipids.
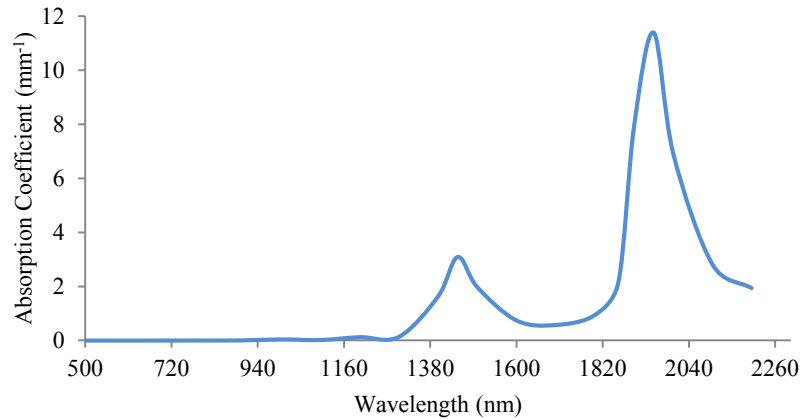
Figure 2.4: The absorption coefficient of water in a wide range of wavelengths between 500 and 2200 nm (Adapted from Hale & Querry 1973).
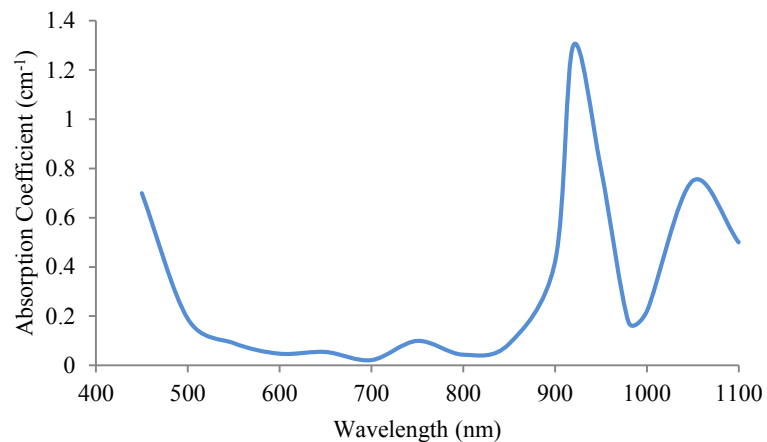
Figure 2.5: The absorption coefficient of lipids in a wide range of wavelengths between 450 and 1100 nm (Adapted from Van et al., 2004).

c) Hemoglobin

Erythrocytes, or red blood cells, contain between 40% and 45% hemoglobin. Hemoglobin plays an important role in oxygen transportation from the lungs to the whole body, and the transportation of waste gases goes back to the lungs. Oxygenated hemoglobin is a state where the hemoglobin is bound with an oxygen molecule. Once the oxygen molecule detach, the hemoglobin is de-oxygenated (Cope 1991). The absorption

spectrum of the oxygenated and deoxygenated hemoglobin differs from each other (Figure 2.6).
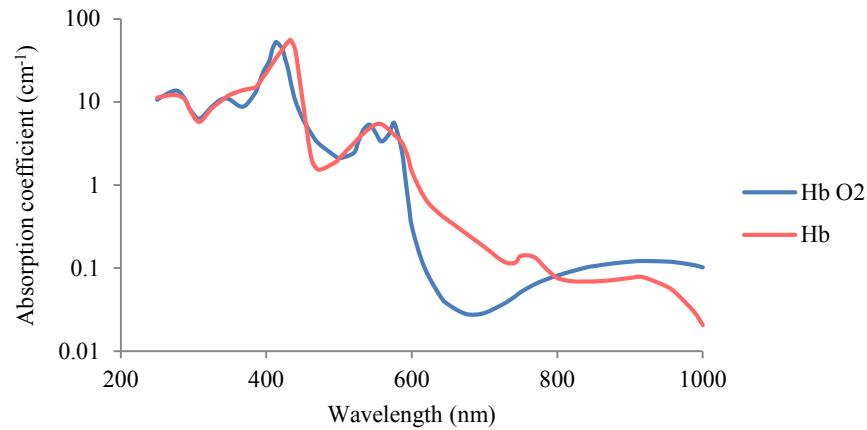
Figure 2.6: The absorption spectrum of hemoglobin between 200 and 1000 nm (Adapted from Cope 1991).

2.3.3 Scattering:

Due to the fact that refractive index of the biological tissue is larger than air (1.35–1.45), some of the incident light is going to reflect on the air/tissue boundaries (Zonios & Dimou 2006). However, the transmitted light that propagates inside the tissue is going to encounter cellular organelles and fluid. The microscopic mismatch of refractive indices of the cellular organelles will cause the light to change its direction. This phenomenon is called scattering. Light scattering depends on the size of the sample, wavelength of light, and the refractive index of the sample (Schmidt 2000).

Scattering coefficient describes the probability of photon scattering per unit path length (mm^{-1}) and it can be calculated by using Lambert-Beer law for a non-absorption medium:

$$I = I_0 \, e^{-\mu_s d} \qquad\qquad \text{Equation (2.3)}$$

where (I) is the light intensity reduced by the scattering, (I_0) is the initiated light intensity, (μ_s) is the scattering coefficient, and (d) is the distance the light traveled in the medium or the thickness of the tissue sample (figure 2.7).
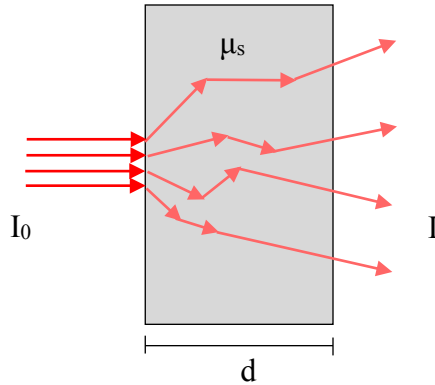
Figure 2.7: The scattering phenomenon. I_o is the incident intensity, I is the final intensity after scattering, d is the thickness, μ_s is the scattering coefficient. The direction of light is going to change during propagation due to refractive mismatch.

2.3.4 Anisotropy Scattering Coefficient (g):

To describe the scattering event, we need first to describe the single scattering phase function P ($\hat{s}', \hat{s}$), where $\hat{s}'$ is the direction of the incident light and $\hat{s}$ is direction of the scattering light. Since the scattering particles are generally considered to be homogeneously distributed within the tissue, we can assume that the scattering depends only on the angle (θ) between $\hat{s}'$ and $\hat{s}$ (Figure 2.8):

$$P (\hat{s}', \hat{s}) = P (\theta) \hspace{4cm} \text{Equation (2.4)}$$

Phase function P ($\hat{s}', \hat{s}$) can be represented by using the anisotropy factor (g). Anisotropy factor (g), defined as the average cosine of scattering angles, determines the probability distribution of scattering angles to the first-order approximation.

$$g = <\cos\theta> = \int_{-1}^{1} p (\cos\theta) \cos\theta \, d (\cos\theta) \hspace{2cm} \text{Equation (2.5)}$$
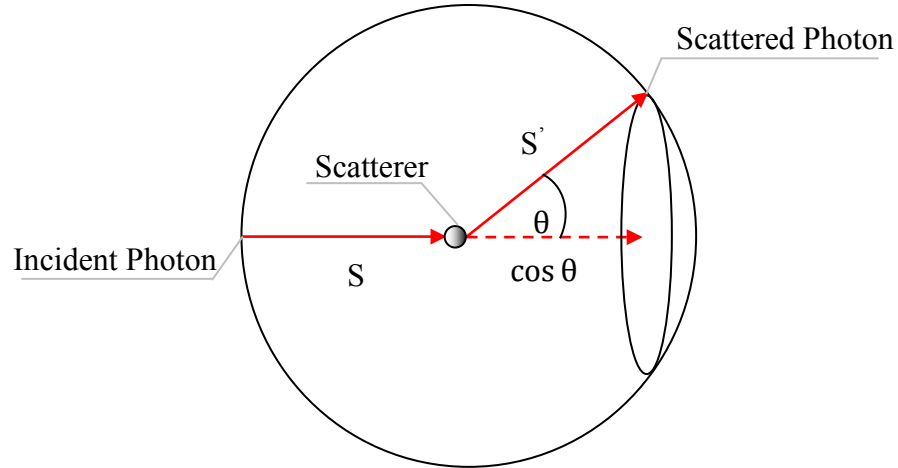
Figure 2.8: Scattering phase function. When a photon hits a scatterer the direction of the light will change. S is the direction of the incident photon, S' is the direction of the scattered photon.

The value of (g) is -1 for backward scattering, 0 unidirectional scattering, and 1 for forward scattering. The typical values of anisotropy coefficient for biological tissue are between 0.7 and 0.9 which means the scattering angle is from 25° to 45°. (Grossweiner, 2005). The most common function used to approximate the phase function is the Henyey-Greenstein phase function:

$$PHG = P\,(\hat{s}', \hat{s}) = \frac{1}{4\pi}\frac{1 - g^2}{(1 + g^2 - 2\,g\cos\theta)^{\frac{3}{4}}}$$
Equation (2.6)

2.4 Light Propagation Models:

When the light hit a turbid tissue, this light is both absorbed and scattered. The scattered light can either transmitted through the tissue or return back to the source due to back-scatter (Figure 2.10). There are number of models used to simulate the propagation of light in the tissue. The most common models are Monte Carlo and adding-doubling.

2.4.1 Monte Carlo Simulation:

The idea behind the Monte Carlo simulation is consecutively launching a huge number of virtual photons into a medium that has absorption and scattering properties and then record either the energy absorbed by the medium or the energy re-emitted from the medium. The photons are initiated with known coordinates, angles‹ and initial weight. The trajectory of the photon can be found by the step size (s):

$$s = -\ln\frac{\xi}{(\mu a + \mu s)} \qquad \text{Equation (2.7)}$$

where s∈ [0, ∞] and ξ is random number in the range of [0,1]. At each step, the photon loses part of its energy due to absorption. The absorption can be described in form of deposited energy (ΔQ):

$$\Delta Q = W\frac{\mu a}{\mu t} \qquad \text{Equation (2.8)}$$

where (W) is the weight of the photon. The new photon weight (ΔW) is found by:

$$\Delta W = W\frac{\mu s}{\mu t} \qquad \text{Equation (2.9)}$$

The deflected angle θ∈ [0, π] can be considered as following:

$$\cos\theta = \frac{1}{g}\left(1 + g^2 - \left(\frac{1 - g^2}{1 - g + 2g\xi}\right)\right) \text{ for } g \neq 0 \qquad \text{Equation (2.10)}$$

After each step, the weight of the photon will reduced until it reaches a certain value. The Monte Carlo then uses a technique called roulette. This technique gives the photon package a chance to survive with a certain weight; otherwise the package is terminated. These calculations will continue until the photon has exited the sample or has terminated.

Monte Carlo simulation is highly flexible and the huge number of photons launched makes this model very accurate. However, Monte Carlo simulation needs both high computational power and time, which can be considered a drawback (Yavari 2006).

2.4.2 Adding-Doubling:

Doubling method assumes that transmission and reflection of a light entering a slab at an angle and exiting at an angle are known for one layer. For an identical thick slab, the transmission and reflection are found by adding the transmission and reflection of each layer. In an arbitrary slab, the transmission and reflection of a thin slab with the same optical properties are calculated by finding the transmission and reflection for a thin slab and then doubling until reaching the desired thickness. For a slab with different optical properties, the adding method is used to extend the doubling method. The transmission and reflection at the boundaries are implemented in the adding doubling method (Prahl et al., 1993).

2.5 Methods for Measuring Optical Properties:

There are number of methods used to measure optical properties. One method is using the integrating sphere system (Figure 2.9). The design of the integrating sphere has some unique features. The inner wall of the integrating sphere is coated with a material that has a nearly 100% diffuse reflectance and minimal absorptive loss. Also, the irradiance on the inner wall of the sphere is uniform. Integrating spheres have at least one port to deliver the light to the tissue sample mounted on the sphere and one port to detect the light within the sphere.

Both single and double integrating sphere can be used. It is preferable to use the double integrating sphere than the single one for its ability to measure both reflectance and transmittance simultaneously (Hlavác 2013). When using double integrating sphere for measuring the optical properties, there is no need to change the position of the tissue sample. The tissue sample is going to be sandwiched between the two integrating spheres. However, the light exchange between the two spheres will make the calibration difficult which is considered a major drawback. In addition, compared to the single sphere, there is more equipment involved in this technique.

In this study we are measuring the optical properties *in-vitro*. There are two ways to determine the optical properties *in-vitro* with the integrating sphere: direct and indirect.

Figure 2.9: The integrating sphere is used to measure the optical properties of a tissue sample.

2.5.1 Direct Method:

Instead of using complicated principles, direct methods use very simple light propagation principles such as Lambert-Beer law. Direct measurement techniques can be used to calculate absorption coefficient (μ_a), scattering coefficient (μ_s), attenuation

coefficient (μ_t), and scattering phase function. Even though these techniques measure the optical properties directly, the major drawback is that these techniques requires a very thin sample such that there is no more than one scattering event (Salas 2007). Creating such sample is difficult for highly scatting media.

2.5.2 Indirect Method:

The *in-vitro* indirect method measures the diffuse reflectance (R_d), diffuse transmittance (T_d), and collimated transmittance (T_c) of the tissue sample first (Figure 2.10). Then, the optical properties (μ_a, μ_s, g) are calculated by using an inverse method relying on either analytical or numerical light propagation models.
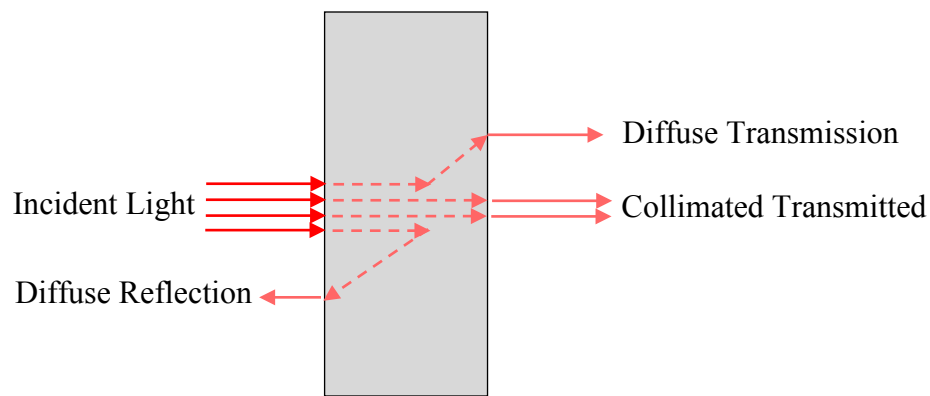
Figure 2.10: The propagation of light through the biological tissue. When a light beam transmits into the tissue it will take into different paths according to its molecular characteristics. Some will transmit through the tissue with some intensity loss due to absorption (Collimated Transmittance) and some will transmit but with a different direction due to scattering (Diffuse Transmission), and some will reflect back due to reflection (Diffuse Reflection).

a) Diffuse Reflection (R_d)

To measure the diffuse reflection (R_d), the tissue sample is mounted on an exit port (Figure 2.11 a). The collimated light goes through the integrating sphere and strikes

the tissue sample. Due to air/tissue refractive index mismatch, some of the light is going to reflect back inside the integrating sphere. The baffle located between the sample and the detector ensures that all light reflected from the sample, either diffusively or reflectively, will strike the integrating sphere at least once before reaching the detector.

b) Diffuse Transmittance (T$_d$)

The diffuse transmittance can be measured by mounting the tissue sample on the entrance port of the integrating sphere (Figure 2.11 b). After the collimated beam hits the tissue sample, some of light is going to change its direction due to scattering. The integrating sphere will capture the unabsorbed scattered beam that transmits through the sample.

c) Collimated Transmittance (T$_c$)

The collimated transmission can be measured by leaving the exit port of the integrating sphere open while the sample is mounted on the entrance port. That will allow the photons that were neither absorbed nor scattered to leave the integrating sphere (Figure 2.11). A second detector located in front of the exit port is going to detect the Collimated Transmittance (T$_c$). This measurement is useful in determining the scattering anisotropy coefficient.
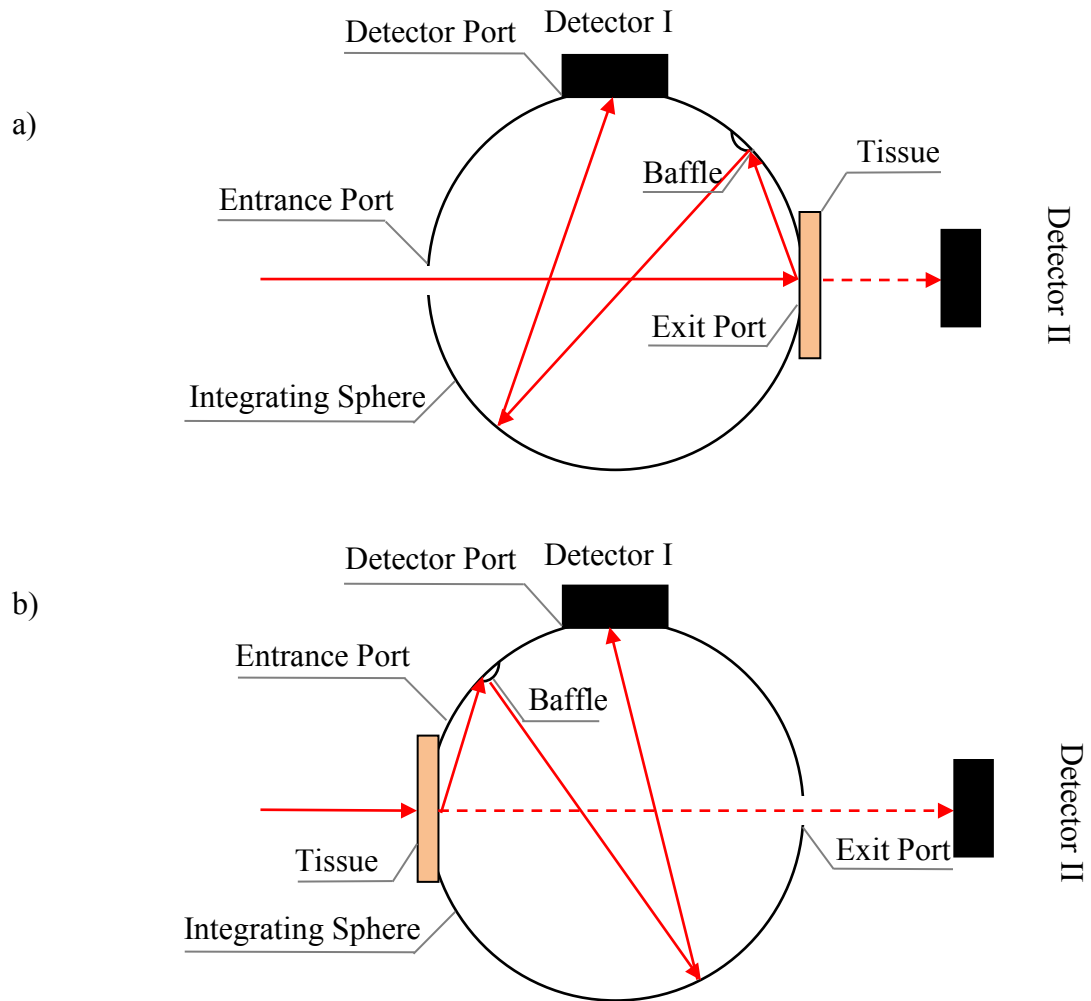
Figure 2.11: a) Diffuse reflection mode where the tissue sample is mounted on the exit port of the integrating sphere. b) Diffuse transmission mode where the tissue sample mounted on the entrance port of the integrating sphere.

Chapter 3: Methods

3.1 General Description:

The optical properties of *in-vitro* rat myocardium and muscle were measured with an indirect technique using a single integrating sphere system (Hammer et al., 1995). The system consists of:

a) Single integrating sphere experimental set-up (Figure 3.1) that measures the diffuse reflection (R_d), diffuse transmission (T_d), and collimated transmission (T_c).

b) Inverse Monte-Carlo light propagation program that calculates the optical parameters (μ_a, μ_s, g) of the tissue sample from the single integrating sphere measurements.
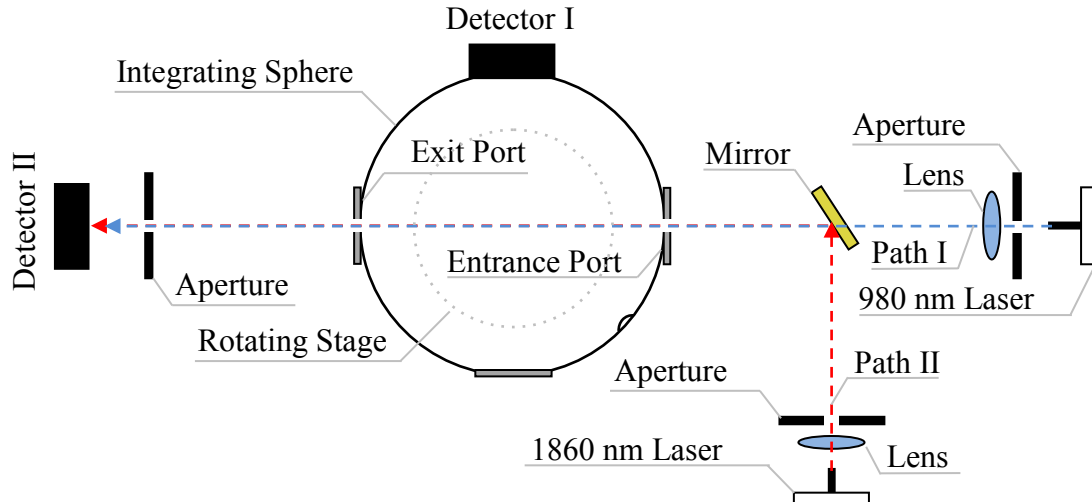
Figure 3.1: A schematic top view of the single integrating sphere system setup. The mirror is mounted on a rotating stage to switch between path I and path II. When the mirror is rotated to 334° the 980 nm CW laser path (Path I) is open. When using the 1860 nm pulsed laser system (Path II) mirror should be rotated back 334° to allow the mirror to reflect the laser beam inside the integrating sphere. The integrating sphere is mounted on a rotating stage as well. The rotating stage gives the ability to the integrating sphere to switch between diffuse transmittance and diffuse reflectance modes.

3.2 Experiment Design:

The general experiment setup is shown in figure 3.1. In this experiment two infrared laser systems were used to measure the optical properties: a 980 nm continuous wave (CW) laser system (AOC5060-1, Applied Optronics, South Plainfield, NJ) and an 1860 nm pulsed laser system (R1870, Lockheed Martin Aculight, Bothell, WA). The two lasers are delivered to the integrating sphere by using an optical fiber. Since there is two laser systems used in this experiment, two paths were designed to deliver each wavelength to the integrating sphere.

The 980 nm laser will be delivered to the system through path I. The lens placed in front of the fiber is going to collimate the laser on entrance port of the integrating sphere. The optical system was designed to produce a beam size less than the diameter of the portholes of the integrating sphere. A circular aperture (Newport Corp., Irvine, CA) is placed between the laser fiber and the lens to reduce the divergence of the incident beam prior to the lens.

The integrating sphere used in this experiment has a diameter of 4 cm (819S-IS-4, Newport Corp., Irvine, CA). To allow easy switching between the diffuse reflection (figure 3.3) and diffuse transmission (figure 3.4) modes, the integrating sphere was mounted on a rotating stage. To measure the light inside the integrating sphere, a photodiode detector (818-SL, Newport Corp., Irvine, CA) is attached to it. The detector is coupled to a power meter (1815-C, Newport Corp., Irvine, CA).

An external photodiode detector (818-SL, Newport Corp., Irvine, CA) is used to detect the collimated beam leaving the integrating sphere through the exit port. The external detector is coupled to a power meter (1815-C, Newport Corp., Irvine, CA). In addition, to prevent scattered light from reaching the detector, a circular aperture

(Newport Corp., Irvine, CA) is placed between the exit port of the integrating sphere and the detector.

When using the 1860 nm laser, the mirror is rotated to 334° to create the second path (path II). Placing the mirror at this particular angle will reflect the light coming out of the fiber and direct it towards the integrating sphere. For 980 nm laser the mirror should be rotated 0° to unblock path I. Since we are using two laser systems in this experiment, the lens and the detectors are not the same. When switching to path II the lens used is compatible with 1860 nm wavelength. The detectors (FIELDMAXII-TOP, COHERENT, Portland, OR) are mounted on the same position shown in figure 3.1. Each of the detectors is coupled to a photometer (FIELDMAXII-TOP, COHERENT, Portland, OR).

3.3 Cell Preparation:

To make the tissue sample cells we used the following protocol (Figure 3.2):

a) A U-shape plastic spacer was cut out of a 50 x 50 mm plastic film. Since, each film is 70μm thick, 8 films were required to form 600μm and 4 films for 300μm.

b) The thickness of the plastic spacer is measured with a caliper.

c) The spacer was glued onto a 50 x 50 mm slide cover glass (B351, Kodak) by using high vacuum grease (DOW CORING Corporation, Midland, MI) while taking care to remove any excess glue. The spacer forms a square frame that will contain the tissue in its center.

d) After sectioning the tissue to the desired thickness with a microtome, the tissue was placed on the glass slide within the plastic frame.

e) Drops of PBS were added on the top of the tissue.

f) The second glass slide was placed on top of the first one to sandwich the tissue in the middle and then slightly compressed to ensure that the plastic spacer is contacted to the glass slides. By doing this step we can ensure that the thickness is uniform across the slide.

3.4 Tissue Preparation:

All measurements were made *in-vitro* using tissue harvested from six adult lab rats. The use of laboratory animals was approved by the University of Miami Animal Care and Use Committee and was in compliance with USDA and NIH Guidelines for the Care and Use of Laboratory Animals. After harvesting the tissues from the euthanized animals, the tissues were kept in a PBS filled containers and stored in a refrigerator. The tissues were then used within the 24 hours to insure that the tissue was fresh.
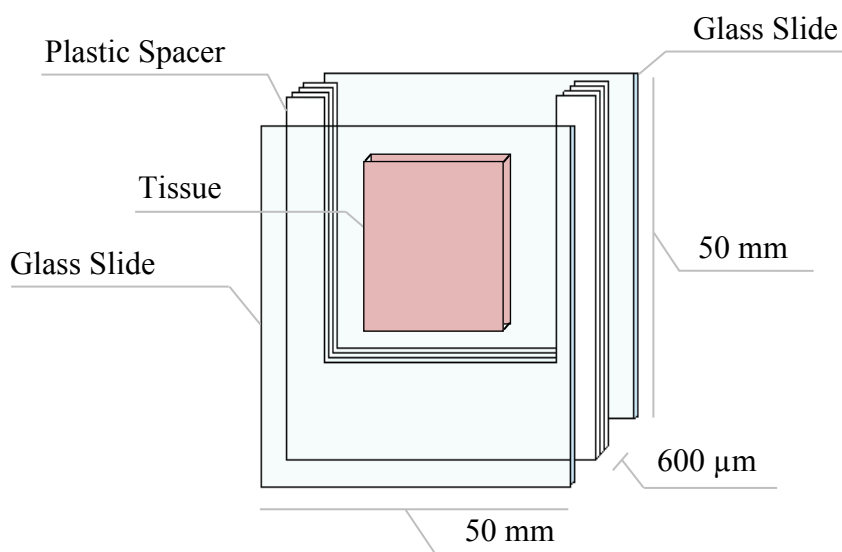
Figure 3.2: The structure of the cell used in the experiment. The sample is sandwiched between two slide glasses. The plastic spacer is used to carry the sample. The whole cell is glued together by using vacuum grease.

A sledge microtome (LEICA SM2400, Heidelberger, Germany) was used to slice the tissue to the desired thickness. After placing the tissue into the fixed holder, we then move the holder back and forth across the cutting knife. For muscle tissue, the sectioning was longitudinal to the muscle fibers. Sectioning the myocardium was parallel to the coronal plane (Figure 3.3).

Apex of heart   Base of heart
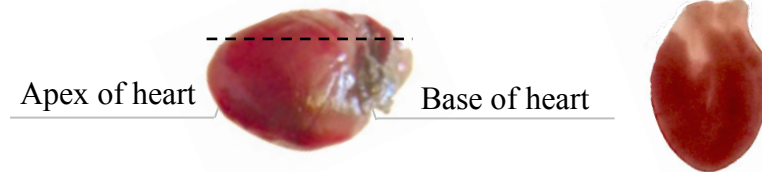
Figure 3.3: A coronal section of the heart.

3.5 Integrating Sphere Measurement Protocol:

3.5.1 Diffuse Transmittance Measurement:

The experiment procedure to measure the diffuse transmittance (Figure 3.4) is the following:

a) The sample is mounted to the entrance port of the integrating sphere by using a sample holder. The rotating stage is placed on 0°.

b) The laser system is turned on.

c) Collimated transmittance light (P_{Tc}) measured by the external detector (Detector II).

d) Diffuse transmittance light (P_{Tcd}) measured by the detector mounted on the integrating sphere (Detector I).

e) Remove the sample form the integrating sphere to measure the incident power (P_{ini-T}) by the external detector (Detector II)
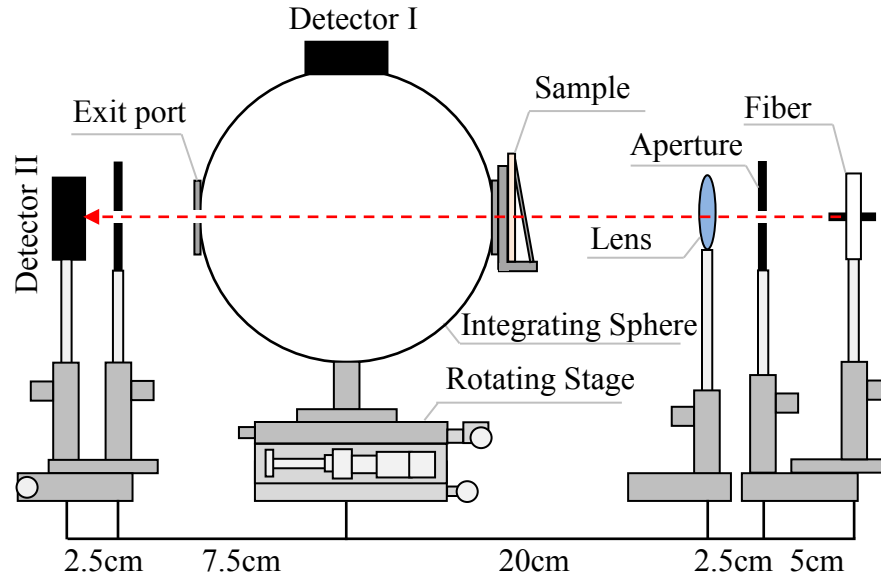
Figure 3.4: The diffuse transmittance mode. The sample is mounted on the exit port of the integrating sphere by using a sample holder. Detector I measures the diffuse transmittance light. The external detector (Detector II) measures the collimated transmittance.

3.5.2 Diffuse Reflectance Measurement:

The experiment procedure to measure the diffuse reflectance (Figure 3.5) is the following:

a) The integrating sphere is rotated 180° so the sample is facing the exit port of the integrating sphere.

b) Collimated transmittance light (P_{Rc}) is measured by the external detector (Detector II).

c) Diffuse reflected light (P_{Rcd}) is measured by the detector mounted on the integrating sphere (Detector I).

d) Remove the sample form the integrating sphere to measure the incident power (P_{ini-R}) by the external detector (Detector II).

Detector I

Sample   Entrance Port   Fiber

Aperture

Detector II

Lens

Integrating Sphere

Rotating Stage

2.5cm   7.5cm   20cm   2.5cm 5cm
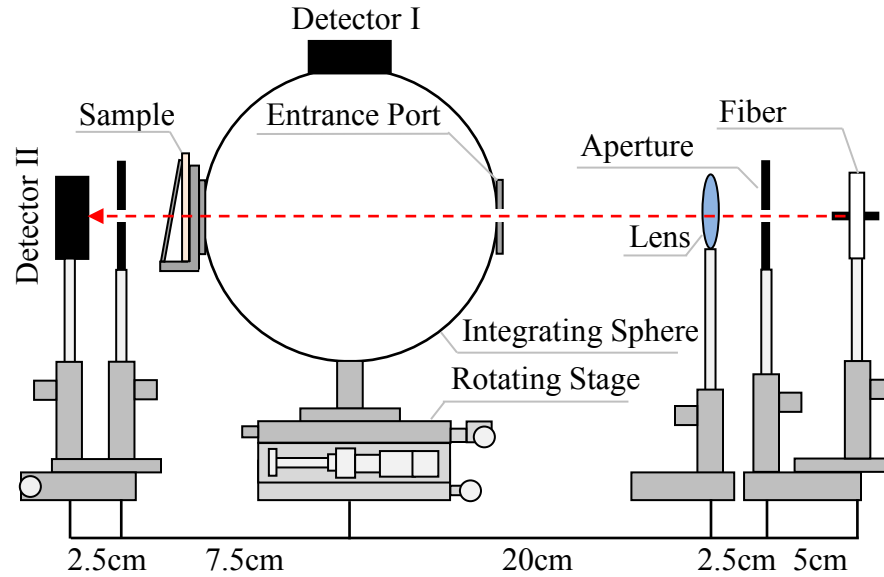
Figure 3.5: The diffuse reflectance mode. The sample is mounted on the exit port of the integrating sphere by using a sample holder. Detector I measures the diffuse reflectance light. The external detector (Detector II) measures the collimated transmittance

3.5.3 Diffuse Irradiance Measurement:

The experiment procedure to measure the diffuse reflectance of the light entering the tissue through the integrating sphere (Figure 3.6) is the following:

a) The sample is moved to the diffuse irradiant port.

b) The exit port of the integrating sphere is closed.

c) Diffuse irradiant light (P_{Rd}) is measured by the detector mounted on the integrating sphere (Detector I).
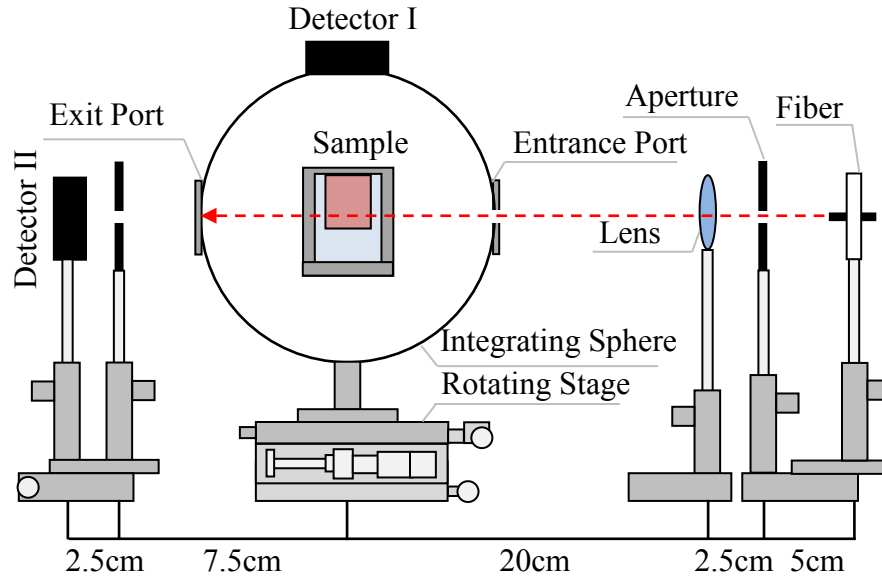
Figure 3.6: The diffuse irradiance mode. The exit port to blocked and the sample is moved to the port facing detector I (diffuse irradiant port). Detector I measures the diffuse irradiation.

3.5.4 Calculating R_{cd}, T_{cd}, and T_c:

After conducting the experiment, the (R_{cd}), (T_{cd}), and (T_c) of a sample can be calculated by using the following equations (Salas 2007):

$$R_{cd} = R \cdot \frac{PRcd}{PRd} \qquad\qquad \text{Equation (3.1)}$$

$$T_{cd} = R \cdot \frac{PTcd}{PRd} \qquad\qquad \text{Equation (3.2)}$$

where (R) is the reflectance of the inner sphere wall provided by the manufacturer. According to the manufacturer's specifications, R is approximately 0.965 for 980 nm laser and 0.98 for 1860 nm laser. P_{Rcd}, P_{Tcd}, and P_{Rd} are obtained from the previous measurements. The collimated transmittance is calculated by using equation 3.3 (Salas 2007).

$$T_c = \left[\frac{P_{Rc}}{P_{in-R}} + \frac{P_{Tc}}{P_{in-T}} \right] / 2 \qquad\qquad \text{Equation (3.3)}$$

After obtaining the (R_{cd}), (T_{cd}), and (T_c) from the previous equations, an inverse Monte Carlo program was used to calculate the optical properties of the sample. However, there are important parameters that should be incorporated into the program. These parameters are the refractive indexes of glass and tissue, beam radii, thickness of the sample, and boundary loss at the sample cell walls.

The boundary loss (K) can be determined experimentally by measuring the collimated transmission for two different sample thicknesses. To calculate the boundary loss (K) the following equation was used:

$$\mu_t = -\ln \frac{\frac{T_c}{K}}{d} \qquad\qquad \text{Equation (3.4)}$$

where (T_c) is the transmission of light through the tissue and the ratio of the output power (P_f) over the input power (P_i), (μ_t) is the attenuation coefficient, (d) represents the thickness of the sample, and (K) is the transmission losses at the sample boundaries.

To simplify the calculations we used 300µm (d_1) and 600µm (d_2) as sample thickness. From equation 3.6:

$$T_{c1} = K\, e^{-\mu_t\, d1} \quad\longrightarrow\quad T_{c1}\,/\,K = e^{-\mu_t\, d1} \qquad\qquad \text{Equation (3.5)}$$

$$T_{c2} = K\, e^{-\mu_t\, d2} \quad\longrightarrow\quad T_{c2}\,/\,K = e^{-\mu_t\, d2} \qquad\qquad \text{Equation (3.6)}$$

Substitute d_1 and d_2 with 300µm and 600µm in equations (3.5) and (3.6) we get the following relationship:

$$T_{c1}\,/\,K = e^{-\mu_t} \qquad\qquad \text{Equation (3.7)}$$

$$T_{c2}\,/\,K = e^{-2\mu_t} \qquad\qquad \text{Equation (3.8)}$$

From equations (3.8) and (3.9):

$$K = T_{c1}^2 /\, T_{c2} \qquad\qquad \text{Equation (3.9)}$$

3.6 Inverse Monte Carlo (IMC) Program:

The Monte Carlo method (see chapter 4) can be designed to simulate the light propagation in the tissue mounted on the optical property measurement system. These simulations can be used to predict the diffuse reflectance (Rd), diffuse transmittance (Td), and collimated transmittance (Tc) of a tissue sample of known optical properties mounted on the integrating sphere. To find the optical properties (μ_a, μ_s, g) from the diffuse reflectance, diffuse transmittance, and collimated transmittance, an inverse method is needed.

IMC sets Initial values of optical properties to calculate the diffuse reflection, diffuse transmittance, and the collimated transmittance through the sample. If the measured values do not match the calculated values, a new set of parameters is used to calculate a new set of R_d, T_d, T_c. This process continues until the measured values match the calculated values within a certain error.

In this study an inverse Monte Carlo program implemented in the MATLAB optimization toolbox (Mathworks, Natick, Massachusetts) was used to determine the optical properties (μ_a, μ_s, and g) of rat muscle and myocardium (Salas 2007). The program was run with these specific inputs:

1. The refractive index (n) of the muscle and myocardium was assumed to be equal to 1.382 (Dirckx et al., 2005).

2. The cell thickness was 600 μm.

3. Beam radius was 1.54 mm.

4. Boundary loss (k) was calculated by using the equation 3.11. The values of K are represented in table 3.1.

5. Defuse reflectance (R_{cd}), defuse transmittance (T_{cd}), and collimated transmittance (T_c) are calculated using equations 3.3, 3.4, and 3.5.

Table 3.1: The Boundary Loss (k) for the Rat Muscle and Myocardium Tissue.

Tissue	λ nm	K
Muscle	980	0.282
	1860	0.412
Myocardium	980	0.532
	1860	0.748

Note. The boundary loss was calculated for both wavelengths (980 and 1860nm) by using equation 3.9

3.7 Integrating Sphere System Validation:

To validate the results of both the single integrating system and the inverse Monte Carlo program, we measured the optical properties of distilled water at 980 nm and 1860 nm and rat liver at 980 nm. Distilled water was used to compare our data with the data from Curcio and Petty (Curcio & Petty, 1951) and we compared the optical properties of the rat liver with the data from Parsa et al (Parsa et al., 1989). The optical properties were measured according to the protocol discussed earlier (Table 4.1).

3.8 Experimental Procedure:

Optical property measurements were performed on six rat myocardium samples and six muscle samples. The average and standard deviation for the μ_a, μ_s, and g for the six samples were calculated. The reduce scattering coefficient ($\mu_s{'}$) for each sample was calculated. The resulting average and standard deviation were calculated for the six

samples of each tissue type. A statistical t-test ($p < 0.05$) was performed between the two

wavelengths for all three optical properties (μ_a, μ_s, and g) and for each tissue type.

Chapter 4: Results

In this chapter we are going to represent the results obtained by the method and materials mentioned in the previous chapter. As what was described earlier, the optical properties were measures by using a single integration sphere and an inverse Monte Carlo program.

4.1 Optical Properties of Distilled Water:

The purpose of using distilled water and liver is to validate and calibrate the method used to measure the optical properties. There was a good agreement between our results, as shown in table 4.1, and the previously published study (Curcio & Petty 1951, Parsa et al 1998). These results made us confident in our method.

Table 4.1: Comparison of the Optical Properties at the Two Wavelengths for Distilled Water and Rat Liver to Previously Published Studies.

Sample	Study	λ nm	$\mu_{a\,(mm^{-1})}$	$\mu_{a\,(mm^{-1})}$	g
Distilled water	Present study	980	0.045	—	—
	Curcio & Petty	980	0.046	—	—
	Present study	1860	2.100	—	—
	Curcio & Petty	1860	2.000	—	—
Rat liver	Present study	980	0.27	6.9	0.94
	Parsa et al.	980	0.62	6.6	0.93

4.2 Optical Properties of Rat Muscle:

The optical properties of the rat muscle are shown in table 4.2. The average absorption coefficient at 980 nm is 0.182 (mm^{-1}) with a standard deviation of 0.0911. At 1860 nm the average absorption coefficient is 1.9785 (mm^{-1}) with a standard deviation of

0.0963. The scattering coefficient is 2.3483 and 1.8341 (mm^{-1}) at 980 nm and 1860 nm with a standard deviation of 0.1969 and 0.2520 respectively. The scattering anisotropy has an average of 0.88 and 0.95 at 980 nm and 1860 nm respectively. Figure 4.1 shows the comparison of the optical properties between the two wavelengths 980 nm and 1860 nm. Statistical analysis where computed by using paired t-test to fiend the relationship between the two wavelengths. The results showed that the absorption coefficient (μ_a) significantly increased at 1860 nm. However, the value of the scattering coefficient (μ_s) decreased significantly at 1860 nm. The computed statistics did not show any significant changes for the anisotropy coefficient (g).

4.3 Optical Properties of Rat Myocardium:

The optical properties of the rat myocardium are shown in table 4.3. The average absorption coefficient at 980 nm is 0.626 (mm^{-1}) with a standard deviation of 0.029. At 1860 nm the average absorption coefficient is 1.637 (mm^{-1}) with a standard deviation of 0.042. The scattering coefficient is 2.7518 and 0.2717 (mm^{-1}) at 980 nm and 1860 nm with a standard deviation of 0.2320 and 0.0345 respectively. The scattering anisotropy has an average of 0.85 and 0.79 at 980 nm and 1860 nm respectively. Figure 4.2 shows the comparison of the optical properties between the two wavelengths 980 nm and 1860 nm. Statistical analysis where computed by using paired t-test to fiend the relationship between the two wavelengths. The results showed that the absorption coefficient (μ_a) and the scattering coefficient (μ_s) significantly increased at 1860 nm. However, the value of the anisotropy coefficient (g) decreased significantly at 1860 nm.

Table 4.2: Optical Properties of Rat Muscle.

λ 980 nm							
Sample	d (μm)	T_c	T_{cd}	R_{cd}	μ_a (mm^{-1})	μ_s (mm^{-1})	g	μ_s' (mm^{-1})
1	600	0.066	0.496	0.056	0.161	2.248	0.90	0.224
2	600	0.058	0.474	0.057	0.231	2.381	0.87	0.309
3	600	0.058	0.414	0.057	0.299	2.321	0.83	0.394
4	600	0.069	0.437	0.059	0.214	2.124	0.84	0.339
5	600	0.054	0.665	0.056	0.029	2.709	0.96	0.108
6	600	0.064	0.517	0.055	0.158	2.307	0.90	0.230
AVG		**0.061**	**0.500**	**0.057**	**0.182**	**2.348**	**0.88**	**0.267**
SD					**0.091**	**0.196**	**0.047**	**0.101**
λ 1860 nm								
Sample	d (μm)	T_c	T_{cd}	R_{cd}	μ_a (mm^{-1})	μ_s (mm^{-1})	g	μ_s' (mm^{-1})
1	600	0.049	0.188	0.003	2.033	1.505	1	0
2	600	0.032	0.186	0.004	1.986	2.226	0.97	0.066
3	600	0.037	0.181	0.003	2.006	1.996	0.99	0.019
4	600	0.046	0.169	0.005	1.830	1.809	0.93	0.126
5	600	0.039	0.142	0.004	2.105	1.802	0.92	0.144
6	600	0.048	0.153	0.004	1.911	1.667	0.92	0.133
AVG		**0.042**	**0.169**	**0.004**	**1.978**	**1.834**	**0.95**	**0.098**
SD					**0.096**	**0.252**	**0.03**	**0.062**
T-test								
T-test					**0.000**	**0.007**	**0.05**	

Note. T_c, T_{cd}, and R_{cd} were obtained from the single integration sphere system. Monte Carlo program was used to calculate μ_a, μ_s, and g. The reduced scattering coefficient ($\mu_s' = \mu_s (1-g)$) was calculated from the measured optical properties.
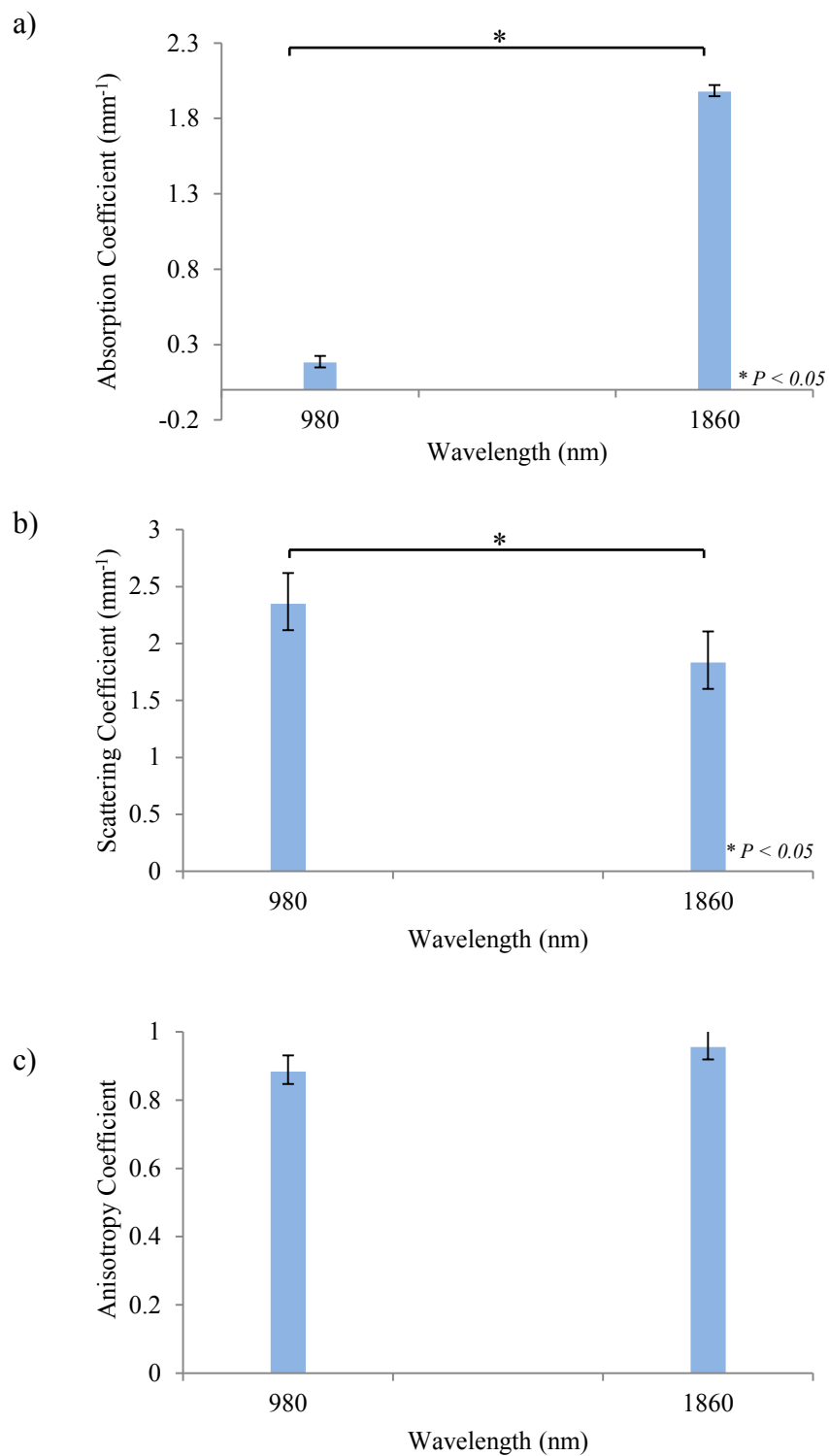
Figure 4.1: Optical properties of the rat muscle. a) absorption, b) scattering, and c) scattering anisotropy.

Table 4.3: Optical Properties of the Rat Myocardium.

λ 980 nm							
Sample	$d_{(\mu m)}$	T_c	T_{cd}	R_{cd}	$\mu_{a\ (mm^{-1})}$	$\mu_{s\ (mm^{-1})}$	g	$\mu_s'_{(mm^{-1})}$
1	600	0.072	0.342	0.032	0.671	2.662	0.85	0.399
2	600	0.069	0.360	0.031	0.640	2.747	0.86	0.384
3	600	0.074	0.362	0.032	0.645	2.622	0.85	0.393
4	600	0.057	0.387	0.036	0.600	3.117	0.87	0.405
5	600	0.085	0.359	0.034	0.585	2.456	0.85	0.368
6	600	0.064	0.387	0.033	0.614	2.904	0.87	0.377
AVG		**0.070**	**0.366**	**0.033**	**0.626**	**2.751**	**0.85**	**0.389**
SD					**0.029**	**0.232**	**0.00**	**0.013**
λ 1860 nm							
Sample	$d_{(\mu m)}$	T_c	T_{cd}	R_{cd}	$\mu_{a\ (mm^{-1})}$	$\mu_{s\ (mm^{-1})}$	g	$\mu_s'\ _{(mm^{-1})}$
1	600	0.048	0.151	0.013	1.680	2.894	0.78	0.636
2	600	0.031	0.165	0.014	1.642	3.659	0.81	0.695
3	600	0.036	0.162	0.014	1.678	3.361	0.80	0.672
4	600	0.046	0.165	0.014	1.572	3.073	0.78	0.676
5	600	0.038	0.160	0.015	1.646	3.316	0.80	0.663
6	600	0.045	0.171	0.013	1.604	3.077	0.82	0.554
AVG		**0.040**	**0.162**	**0.014**	**1.637**	**3.230**	**0.79**	**0.651**
SD					**0.042**	**0.271**	**0.01**	**0.050**
T-test							
T-test					**0.000**	**0.034**	**0.00**	

Note. T_c, T_{cd}, and R_{cd} were obtained from the single integration sphere system. Monte Carlo program was used to calculate μ_a, μ_s, and g. The reduced scattering coefficient ($\mu_s' = \mu_s (1-g)$) was calculated from the measured optical properties.
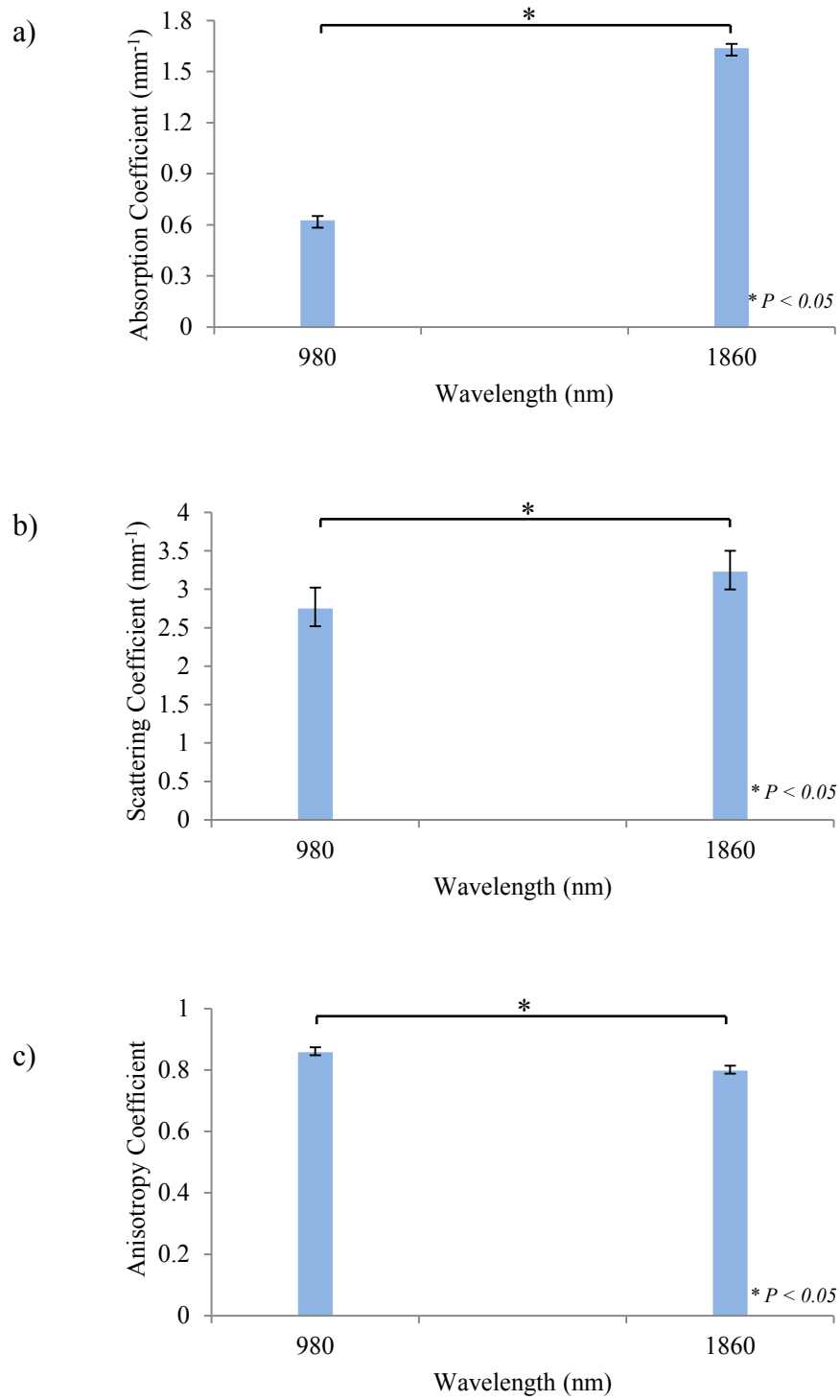
Figure 4.2: Optical properties of rat myocardium. a) absorption coefficient b) scattering coefficient and c) scattering anisotropy.

Chapter 5: Discussion

In this study, the optical properties of the rat muscle and myocardium were measured at 980 and 1860 nm. The measurements were performed *in-vitro* using a single integrating sphere system. These measurements were used to calculate the diffuse transmission, diffuse reflection, and collimated transmission. The optical properties were obtained from these three measurements using an inverse Monte Carlo program.

5.1 Optical Properties of Muscle and Myocardium for Different Animals:

The optical properties of biological tissues have been published at a wide range of wavelengths. Yet, to the best of our knowledge, there are no published data about the optical properties of either rat muscle or myocardium at 1860 nm. Due to this, we cannot compare the results we obtained with others. However, for 980 nm the available data showed differences between our results and the literature (Table 5.1). The measurement of optical properties depends on both tissue preparation and the method used to calculate these properties. Thus, a large variation in optical properties can be found between different studies. For example, the absorption coefficient (μ_a) at 650 nm was 0.056 mm^{-1} at Nilsson et al and 0.14 at Han et al.

The available data for myocardium optical properties are found in table 5.2. Comparing the results of our study with the one in the literature, we still can see some differences but not as large as in muscle. At 1000 nm, the absorption coefficient was 0.4 mm^{-1} at Schwarzmaier et al and at 980 nm was 0.626 mm^{-1} in our study. Even though an inverse Monte Carlo simulation has been used in both studies, the tissue used was taken from different animals and that might cause these differences.

Table 5.1: The Optical Properties of Muscle in Different Animals.

Tissue	Species	λ nm	μ$_{a}$ mm^{-1}	μ$_{s}$ mm^{-1}	g	Author
Muscle	Rabbit	630	0.14	11	0.84	Beek et al., 1997
	Piglet	630	0.120	23.9	0.73	Beek et al., 1997
	Rabbit	633	0.074	14	0.96	Beek et al., 1997
	Piglet	632.8	0.059	17.9	0.85	Beek et al., 1997
	Rabbit	790	0.230	15.7	0.95	Beek et al., 1997
Muscle	Rat	500	0.117	8.92	0.90	Nilsson et al., 1995
	Rat	550	0.166	8.82	0.90	Nilsson et al., 1995
	Rat	600	0.095	8.33	0.92	Nilsson et al., 1995
	Rat	650	0.056	7.9	0.93	Nilsson et al., 1995
	Rat	700	0.052	7.367	0.93	Nilsson et al., 1995
	Rat	750	0.052	7.13	0.93	Nilsson et al., 1995
	Rat	800	0.054	6.67	0.93	Nilsson et al., 1995
Muscle	Rat	450	0.5	—	0.84	Han et al., 2006
	Rat	500	0.3	—	0.82	Han et al., 2006
	Rat	550	0.23	—	0.82	Han et al., 2006
	Rat	600	0.16	—	0.81	Han et al., 2006
	Rat	650	0.14	—	0.79	Han et al., 2006
Muscle	Beef	500	0.149	—	—	Xia et al., 2007
	Beef	550	0.143	—	—	Xia et al., 2007
	Beef	600	0.193	—	—	Xia et al., 2007
	Beef	650	0.041	—	—	Xia et al., 2007
	Beef	700	0.016	—	—	Xia et al., 2007
	Beef	750	0.011	—	—	Xia et al., 2007
	Beef	800	0.009	—	—	Xia et al., 2007
	Beef	850	0.011	—	—	Xia et al., 2007
	Beef	900	0.015	—	—	Xia et al., 2007
	Beef	950	0.026	—	—	Xia et al., 2007

Tissue	Species	λ nm	μ_a mm^{-1}	μ_s mm^{-1}	g	Author
Muscle	Turkey	850	0.02	7.0	0.94	Roggan et al., 1995
	Turkey	1064	0.04	8.0	0.98	Roggan et al., 1995
	Canine	1064	0.04	18.0	0.96	Roggan et al., 1995
	Bovine	1064	0.03	14.0	0.96	Roggan et al., 1995
	Porcine	1064	0.03	13.0	0.96	Roggan et al., 1995
Muscle	Human	1064	0.04	25.0	0.94	Roggan et al., 1995
	Human	650	0.133	—	—	Simpson et al., 1998
	Human	700	0.052	—	—	Simpson et al., 1998
	Human	750	0.044	—	—	Simpson et al., 1998
	Human	800	0.024	—	—	Simpson et al., 1998
	Human	850	0.033	—	—	Simpson et al., 1998
	Human	900	0.039	—	—	Simpson et al., 1998
	Human	950	0.052	—	—	Simpson et al., 1998
	Human	1000	0.057	—	—	Simpson et al., 1998

Table 5.2: The Optical Properties of Myocardium in Different Animals.

Tissue	Animal	λ nm	μ_a mm^{-1}	μ_s mm^{-1}	g	Author
Myocardium	Dog	630	0.20	15.9	0.85	Beek et al., 1997
	Dog	632.8	0.21	19.1	0.94	Beek et al., 1997
	Dog	790	0.09	16.4	0.94	Beek et al., 1997
Myocardium	Bovine	1000	0.24	8.6	0.93	Schwarzmaier et al., 1998
	Bovine	1100	0.23	8.2	0.93	Schwarzmaier et al., 1998
	Bovine	1200	0.32	7.7	0.94	Schwarzmaier et al., 1998
	Bovine	1300	0.31	7.3	0.93	Schwarzmaier et al., 1998
	Bovine	1400	0.72	6.9	0.91	Schwarzmaier et al., 1998
	Bovine	1500	1.01	6.8	0.87	Schwarzmaier et al., 1998

5.2 Optical Properties:

Muscle tissue consists of small fibers, blood vessels, and nerves. In addition, muscle cell contains intracellular organelles, plasma, water, etc. These different structures will contribute in the optical properties (absorption and scattering).

5.2.1 Absorption Coefficient (μ_a):

According to our results (Table 5.2), rat myocardium the light absorption is significantly higher at 1860 nm (1.637 ± 0.042 mm^{-1}) than at 980 nm (0.6263 ± 0.032 mm^{-1}). The absorption coefficient at 1860 nm is (1.9785 ± 0.096 mm^{-1}) and at 980 nm is (0.182 ± 0.091 mm^{-1}).

To the best of our knowledge, there is no available data for 1860 nm and 980 nm to compare with. Even if there were, it would be difficult to compare the results of two studies. The variation of tissues, thickness of each sample, and the preparation conditions will effect the optical properties measurements. Moreover, the method used (*in-vivo* and *ex-vivo,* direct and indirect) also affects the results. These changes, even if it was slight, will reflect on the results.

Looking at the optical properties of the rat myocardium (Figure 5.1), we can see clearly that the average absorption coefficient (μ_a) at 1860 nm is higher than at 980 nm by the factor of 2.6. For rat muscle, the average absorption coefficient (μ_a) at 1860 nm is higher than at 980 nm by a factor of 10.8. Around 71.98% of muscle tissue is water (Rajanayagam et al., 1991) and it is known that the water is considered the main chromophore in the IR region. Therefore, according to the trend seen by the absorption spectrum of water (Hale & Querry 1973), we can say that the elevation in absorption is

due to water. Not only muscle and myocardium have a higher absorption at 1860 nm, also the liver tissue (Parsa, et al., 1989) is following the same trend (Figure 5.1).
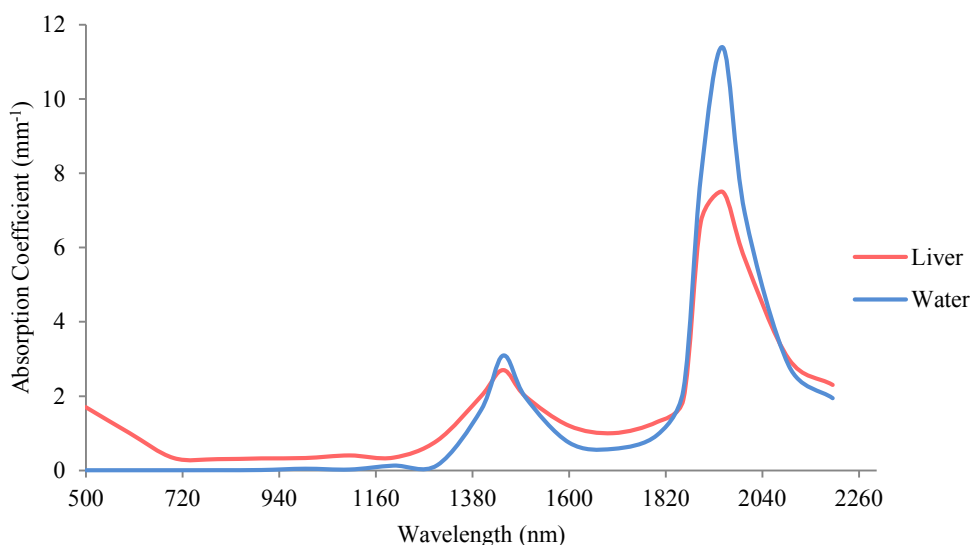

Figure 5.1: The absorption coefficient of a rat liver (red) and water (blue) in a wide range of wavelengths between 500 and 2200 nm. There are two distinguished peaks in the IR region at 1420 and 1940 nm. The absorption coefficient of rat liver was adapted from (Parsa, et al., 1989). The absorption coefficient of water was adapted from (Hale & Querry 1973).

Moreover, At 980 nm the absorption coefficient of muscles ~ 0.182 /mm and myocardium ~1.978/mm was significantly higher that the absorption coefficient of water ~ 0.045/mm. The increase in absorption can be explained by the absorption spectrum of a secondary chromophore found in the mitochondria called cytochrome c oxidase. Cytochrome c oxidase is considered as an initial absorption site in the visible-to-near IR optical region (Karu et al., 2005). However, at 1863 nm the absorption coefficient of muscle ~1.973/mm and myocardium ~1.637/mm was lower than water ~2.00/mm. Due to the fact that muscle contains around 71.98% water, a secondary effect of photothermal driven by the mitochondria is possible because they contain most of the cellular chromophores (Salet et al., 1987).

5.2.2 Scattering Coefficient (μ_s):

The main reason for light scattering is the difference in refraction index between the two mediums. In any biological tissue, the main scattering media are found in both intra and extra cellular spaces. Also, the cell nucleus and organelles contribute in light scattering phenomenon. In the previous chapter, we found that the scattering coefficient (μ_s) for rat's myocardium at 1860 nm is slightly higher than 980 nm by a factor of 1.17. For muscles, the scattering coefficient (μ_s) at 1860 nm is 78% lower than 980 nm.

5.2.3 Anisotropy Coefficient (g):

In table 4.2, the anisotropy coefficient (g) for rat's myocardium at 980nm is significantly higher than 1860nm. For muscles, there is a slight increasing in the anisotropy coefficient (g) at 1860 nm than 980 nm. According to these numbers, the anisotropy coefficient is considered as a forward scattering (anisotropic) and the values are lying between the range 0.7 and 0.9.

5.3 Limitations:

To avoid potential errors and to obtain accurate results in this study, numbers of potential errors were considered. When using the single integrating sphere system, we assured that the incident light is highly collimated by using apertures on both the fiber and detector. Even though the intensity of the light at that point was reduced, we obtained a highly collimated beam.

By using a single integrating sphere system, the tissue sample was moved around the sphere to obtain all three measurements. Thus, it was important to make sure that the tissue sample is accurately positioned to the laser beam before taking the measurements.

The tissues can be considered a source of error if they are not prepared properly. In any biological investigation, it is important to understand that any changes in the tissue (enzymatic processes or autolysis) can cause a change on the measurements and that will reflect on their optical properties. Another important factor is the size and thickness of the sample. If the tissue is too thick, it will cause an increase in signal to noise ratio.

5.4 Future Work:

Due to the lack of information about the optical properties of muscles and myocardium at 1860 nm, the areas that seem to us worth investigation are the contribution of the mitochondrial chromophores of that particular wavelength. Also, the optical properties being measured *in-vitro* did not take under consideration some factors like the lack of blood in the tissue, the time between tissue harvesting and measurement, and the use of PBS for rehydration the tissue. Thus, measuring the optical properties of the tissue *in-vivo* is needed to get more accurate results.

REFERENCES

Adams, S. R., & Tsien, R. Y. (1993). Controlling cell chemistry with caged compounds. *Annual Review of Physiology*, *55*(1), 755–784.

Arvanitaki, A., & Chalazonitis, N. (1961). *Excitatory and inhibitory processes initiated by light and infra-red radiations in single identifiable nerve cells (giant ganglion cells of Aplysia)*. Oxford, England: Pergamon Press.

Bear, M. F., Connors, B. W., & Paradiso, M. A. (Eds.). (2007). *Neuroscience* (3rd ed.). Baltimore, MD: Lippincott, Williams, & Wilkins.

Beek, J. F., Blokland, P., Posthumus, P., Aalders, M., Pickering, J. W., Sterenborg, H. J. C. M., & Van Gemert, M. J. C. (1997). In vitro double-integrating-sphere optical properties of tissues between 630 and 1064 nm. *Physics in Medicine and Biology*, *42*(11), 2255–2261.

Cheong, W. F., Prahl, S. A., & Welch, A. J. (1990). A review of the optical properties of biological tissues. *IEEE Journal of Quantum Electronics*, *26*(12), 2166–2185.

Conway, J. M., Norris, K. H., & Bodwell, C. E. (1984). A new approach for the estimation of body composition: Infrared interactance. *American Journal of Clinical Nutrition*, *40*(6), 1123–1130.

Cope, M. (1991). *The development of a near infrared spectroscopy system and its application for noninvasive monitoring of cerebral blood and tissue oxygenation in the newborn infants* (Doctoral dissertation). University of London, England.

Curcio, J. A., & Petty, C. C. (1951). The near infrared absorption spectrum of liquid water. *Journal of the Optical Society of America*, *41*(5), 302–302.

Dirckx, J. J., Kuypers, L. C., & Decraemer, W. F. (2005). Refractive index of tissue measured with confocal microscopy. *Journal of Biomedical Optics*, *10*(4), 044014-044014.

Dittami, G. M., Rajguru, S. M., Lasher, R. A., Hitchcock, R. W., & Rabbitt, R. D. (2011). Intracellular calcium transients evoked by pulsed infrared radiation in neonatal cardiomyocytes. *Journal of Physiology*, *589*(6), 1295–1306.

Evans, D. H., & Abrahamse, H. (2008, October). *Effect of laser irradiation on mitochondrial responses of stressed keratinocytes*. Paper presented at the International Conference of the World Association of Laser Therapy, Sun City, North West Province, South Africa. Retrieved from http://www.biolase.com /Medical/Documents/Effect-of-Laser-Irradiation-on-Mitochondrial.pdf

Fork, R. L. (1971). Laser stimulation of nerve cells in Aplysia. *Science*, *171*(3974), 907–908.

Gonzalez-Lima, F., Barksdale, B. R., & Rojas, J. C. (2014). Mitochondrial respiration as a target for neuroprotection and cognitive enhancement. *Biochemical Pharmacology*, *88*(4), 584–593.

Grossweiner, L. I. (2005). *The science of phototherapy: An introduction*. Dordrecht, Netherlands: Springer.

Hale, G. M., & Querry, M. R. (1973). Optical constants of water in the 200-nm to 200-µm wavelength region. *Applied Optics*, *12*(3), 555–563.

Hammer, M., Roggan, A., Schweitzer, D., Müller, G. (1995). Optical properties of ocular fundus tissues-an in vitro study using the double integrating-sphere technique and inverse Monte Carlo simulation. *Physics in Medicine and Biology*, *40*, 963–978.

Han, Y. H., Yang, J. M., Yoo, J. S., Ogay, V., Kim, J. D., Kim, M. S., . . . Lee, B. C. (2006). Measurement of the optical properties of in-vitro organ-surface Bonghan corpuscles of rats. *Journal of the Korean Physical Society*, *49*(6), 2239–2246.

Hirase, H., Nikolenko, V., Goldberg, J. H., & Yuste, R. (2002). Multiphoton stimulation of neurons. *Journal of Neurobiology*, *51*(3), 237–247.

Hlavác, B. M. (2013). *Measurement of tissue optical properties*. Czech Technical University, Prague, Faculty of Electrical Engineering, Department of Cybernetics.

Hollis, V. S. (2002). *Non-invasive monitoring of brain tissue temperature by near-infrared spectroscopy* (Doctoral dissertation). University College, London, England.

Izzo, A. D., Richter, C. P., Jansen, E. D., & Walsh, J. T. (2006). Laser stimulation of the auditory nerve. *Lasers in Surgery and Medicine*, *38*(8), 745–753.

Jacques, S. L. (1992). Laser-tissue interactions. Photochemical, photothermal, and photomechanical. *Surgical clinics of North America*, *72*(3), 531–558.

Karu, T. I., (2014) Cellular and molecular mechanisms of photobiomodulation (low-power laser therapy). *Selected Topics in Quantum Electronics*, *20*(2), 143–148.

Karu, T. I., Pyatibrat, L. V., Kolyakov, S. F., & Afanasyeva, N. I. (2005). Absorption measurements of a cell monolayer relevant to phototherapy: Reduction of cytochrome c oxidase under near IR radiation. *Journal of Photochemistry and Photobiology B: Biology*, *81*(2), 98–106.

Kandel, E. R., Schwartz, J. H., & Jessell, T. M. (Eds.). (2000). *Principles of neural science* (Vol. 4). New York, NY: McGraw-Hill.

McGovern, B., Berlinguer Palmini, R., Grossman, N., Drakakis, E., Poher, V., Neil, M. A. A., & Degenaar, P. (2010). A new individually addressable micro-LED array for photogenetic neural stimulation. *Biomedical Circuits and Systems*, *4*(6), 469–476.

Nilsson, A. M., Berg, R., & Andersson-Engels, S. (1995). Measurements of the optical properties of tissue in conjunction with photodynamic therapy. *Applied Optics*, *34*(21), 4609–4619.

Parent, A. (2004). Giovanni Aldini: From animal electricity to human brain stimulation. *Canadian Journal of Neurological Sciences*, *31*(4), 576–584.

Parsa, P., Jacques, S. L., & Nishioka, N. S. (1989). Optical properties of rat liver between 350 and 2200 nm. *Applied Optics*, *28*(12), 2325–2330.

Prahl, S. A., van Gemert, M. J., & Welch, A. J. (1993). Determining the optical properties of turbid mediaby using the adding–doubling method. *Applied Optics*, *32*(4), 559–568.

Rajguru, S. M., Matic, A. I., & Richter, C. P. (2010). Optical stimulation of neurons. In F. S. Pavone (Ed.), *Laser imaging and manipulation in cell biology* (pp. 99–112). Hoboken, NJ: Wiley.

Roggan, A., Albrecht, H. J., Doerschel, K., Minet, O., & Mueller, G. J. (1995, January). *Experimental set-up and Monte-Carlo model for the determination of optical tissue properties in the wavelength range 330 to 1100 nm*. Paper presented at the International Symposium on Biomedical Optics, Europe.

Roggan, A., Dörschel, K., Minet, O., Wolff, D., & Müller, G. (1995, June). *The optical properties of biological tissue in the near infrared wavelength range: Review and measurements*. Paper presented at the Annual Meeting of the International Society for Optical Engineering, Berlin, Germany.

Rajanayagam, V., Fabry, M. E., & Gore, J. C. (1991). In vivo quantitation of water content in muscle tissues by NMR imaging. *Magnetic Resonance Imaging*, *9*(4), 621–625.

Salas, N. (2007). *Development of a delivery system and optical-thermal model for laser interstitial thermotherapy of breast tumors* (Doctoral dissertation). Retrieved from http://scholarlyrepository.miami.edu/oa_dissertations/20/

Salet, C., Passarella, S., & Quagliariello, E. (1987). Effects of selective irradiation on mammalian mitochondria. *Photochemistry and Photobiology*, *45*(3), 433–438.

Schmidt, F. E. W. (2000). *Development of a time-resolved optical tomography system for neonatal brain imaging* (Doctoral dissertation). University of London, England.

Schwarzmaier, H. J., Yaroslavsky, A. N., Terenji, A., Willmann, S., Yaroslavsky, I. V., & Kahn, T. (1998, May). Changes in the optical properties of laser-coagulated and thermally coagulated bovine myocardium. *Proceedings of SPIE: The International Society for Optics and Photonics*, *3254*, 361–365. doi:10.1117/12.308186

Simpson, C. R., Kohl, M., Essenpreis, M., & Cope, M. (1998). Near-infrared optical properties of ex vivo human skin and subcutaneous tissues measured using the Monte Carlo inversion technique. *Physics in Medicine and Biology*, *43*(9), 2465–2478.

Sørensen Dam, J. (2000). *Optical analysis of biological media-continuous wave diffuse spectroscopy* (Doctoral thesis). Lund University, Lund, Sweden.

Thomsen, S. (1991). Pathologic analysis of photothermal and photomechanical effects of laser–tissue interactions. *Photochemistry and Photobiology*, *53*(6), 825–835.

van Veen, R. L., Sterenborg, H. J. C. M., Pifferi, A., Torricelli, A., & Cubeddu, R. (2004, April). *Determination of VIS-NIR absorption coefficients of mammalian fat, with time-and spatially resolved diffuse reflectance and transmission spectroscopy*. Paper presented at the Conference of the Optical Society of America.

Wade, P. D., Taylor, J., & Siekevitz, P. (1988). Mammalian cerebral cortical tissue responds to low-intensity visible light. *Proceedings of the National Academy of Sciences*, *85*(23), 9322–9326.

Welch, A. J., & Gemert, M. J. C. (2011). *Optical-thermal response of laser-irradiated tissue* (2nd ed.). London, England: Springer.

Wells, J., Kao, C., Konrad, P., Milner, T., Kim, J., Mahadevan-Jansen, A., & Jansen, E. D. (2007). Biophysical mechanisms of transient optical stimulation of peripheral nerve. *Biophysical Journal*, *93*(7), 2567–2580.

Wells, J., Kao, C., Mariappan, K., Albea, J., Jansen, E. D., Konrad, P., & Mahadevan-Jansen, A. (2005). Optical stimulation of neural tissue in vivo. *Optics Letters*, *30*(5), 504–506.

White, D. R., Widdowson, E. M., Woodard, H. Q., & Dickerson, J. W. T. (1991). The composition of body tissues. (II) Fetus to young adult. *British Journal of Radiology*, *64*(758), 149–159.

Xia, J. J., Berg, E. P., Lee, J. W., & Yao, G. (2007). Characterizing beef muscles with optical scattering and absorption coefficients in VIS-NIR region. *Meat Science*, *75*(1), 78–83.

Yavari, N. (2006). *Optical spectroscopy for tissue diagnostics and treatment control* (Doctoral thesis). University of Bergen, Norway.

Zonios, G., & Dimou, A. (2006). Modeling diffuse reflectance from semi-infinite turbid media: Application to the study of skin optical properties. *Optics Express*, *14*(19), 8661−8674.